Productive infection of the retinal pigment epithelium by SARS-CoV-2: Initial effects and consideration of long-term consequences

Nan W. Hultgren [a,*], Anton Petcherski [b], Simona Torriano[a], Ravikiran Komirisetty[a], Madhav Sharma[b], Tianli Zhou[a], Barry L. Burgess [a], Jennifer Ngo [b], Corey Osto[b], Byourak Shabane [b], Orian S. Shirihai[b,c], Theodoros Kelesidis [b,d] and David S. Williams [a,e,*]

[a]Department of Ophthalmology and Stein Eye Institute, University of California, Los Angeles, CA 90095, USA
[b]Department of Medicine, David Geffen School of Medicine, University of California Los Angeles, Los Angeles, CA 90095, USA
[c]Department of Molecular and Medical Pharmacology, University of California, Los Angeles, CA 90095, USA
[d]Department of Internal Medicine, University of Texas Southwestern Medical Center, Dallas, TX 75390, USA
[e]Department of Neurobiology, David Geffen School of Medicine; Molecular Biology Institute; Brain Research Institute, University of California, Los Angeles, CA 90095, USA
*To whom correspondence should be addressed: Email: nanwu36@g.ucla.edu (N.W.H.); dswilliams@g.ucla.edu (D.S.W.)
Edited By Ivet Bahar

Abstract

As the SARS-CoV-2 coronavirus continues to evolve and infect the global population, many individuals are likely to suffer from post-acute sequelae of SARS-CoV-2 infection (PASC). Manifestations of PASC include vision symptoms, but little is known about the ability of SARS-CoV-2 to infect and impact the retinal cells. Here, we demonstrate that SARS-CoV-2 can infect and perturb the retinal pigment epithelium (RPE) in vivo, after intranasal inoculation of a transgenic mouse model of SARS-CoV-2 infection, and in cell culture. Separate lentiviral studies showed that SARS-CoV-2 Spike protein mediates viral entry and replication in RPE cells, while the Envelope and ORF3a proteins induce morphological changes. Infection with major variants of SARS-CoV-2 compromised the RPE barrier function and phagocytic capacity. It also caused complement activation and production of cytokines and chemokines, resulting in an inflammatory response that spread across the RPE layer. This inflammatory signature has similarities to that associated with the onset of age-related macular degeneration (AMD), a major cause of human blindness, resulting from RPE pathology that eventually leads to photoreceptor cell loss. Thus, our findings suggest that post-acute sequelae of SARS-CoV-2 infection of the RPE may have long-term implications for vision, perhaps comparable to the increased occurrence of AMD found among individuals infected by HIV, but with greater public health consequences due to the much larger number of SARS-CoV-2 infections.

Keywords: retinal pigment epithelium, complement activation, SARS-CoV-2 virus, long-COVID, age-related macular degeneration

---

Significance Statement

SARS-CoV-2 continues to infect humans worldwide, with a variety of symptoms, including neurological symptoms, occurring long beyond the acute phase of infection. Little is understood about the ability of SARS-CoV-2 to infect and impact the retina. Here, we demonstrate that different variants of SARS-CoV-2 can efficiently and productively infect the retinal pigment epithelium (RPE), cause cellular damage, and compromise RPE functions. SARS-CoV-2 infection also induced an inflammatory response that spread across the RPE and sub-RPE layers and is comparable to the underlying RPE pathology reported for age-related macular degeneration, in which RPE impairment eventually leads to photoreceptor damage and loss of central eyesight. Thus, SARS-CoV-2 infection of the RPE may have a significant long-term impact on vision.

Introduction

Although hospitalization rates and mortalities resulting from severe COVID-19 have declined significantly (1–3), infection and re-infection with SARS-CoV-2 variants persist, and there are numerous reports of post-acute sequelae of SARS-CoV-2 infection (PASC or long-COVID) (4–6). Notably, viral neuroinvasion can lead to several neurological symptoms characteristic of PASC, including visual impairment, loss of smell or taste, "brain fog," headaches, and other neurocognitive sequelae (7). Mechanisms of neuroinvasion of SARS-CoV-2 and associated brain damage include entry of SARS-CoV-2 through binding with the host cell receptor, ACE2, and utilization of host proteases like TMPRSS2 or

olfactory retrograde trans-synaptic and vascular routes of viral neuroinvasion (8). However, a somewhat overlooked area in the pathogenesis of SARS-CoV-2 infection is the infection of the eye, particularly the retinal cells, and the potential long-term effects on vision. The retina is part of the central nervous system, and SARS-CoV-2 has been shown to infect primary human retinal cells (9) and human retinal organoids in vitro (10). However, little is known about the ability of different SARS-CoV-2 variants of concern (VOC) to infect retinal cells and how they might impact their long-term function.

Experimental animal studies have shown that other coronaviruses can infect various retinal cell types regardless of the inoculation route, and the infection elicits both acute and long-lasting negative effects on the retina, causing damage to both the photoreceptors and the RPE (11–13). The SARS-CoV-2 receptor ACE2 has been shown to be expressed by the human RPE (9, 14), making it a potential target cell type for SARS-CoV-2 infection. The vascularization of the mammalian retina is supported by both the inner retinal vessels and the choroid (15). Although located in the posterior chamber of the eye, the retina is still accessible to SARS-CoV-2, especially in the setting of viremia during COVID-19 (16). Both SARS-CoV-2 viral protein and RNA have been detected in human patient retinal tissue samples (17–19). A very recent study, published during the preparation of this manuscript, demonstrated that wild-type (WT) SARS-CoV-2 virus can reach and infect both the anterior and the posterior chamber of the eye following intranasal inoculation in a human ACE2 transgenic mouse model (20). However, the presence of SARS-CoV-2 and its productive infection of the RPE has not been clearly demonstrated.

The RPE plays a critical role in maintaining photoreceptor function (21). An impaired RPE precedes the loss of photoreceptor function in most macular degenerations (22, 23). Therefore, SARS-CoV-2 infection in the RPE could pose a detrimental long-term effect on the outer retinal health, possibly contributing to changes in vision reported in individuals ~6 months post-acute infection (24), but perhaps more likely on an even longer timescale. Of significance is that activation of complement and inflammasome pathways is associated with SARS-CoV-2 infection (25, 26) and is also involved in age-related macular degeneration (AMD) (27), the main cause of visual impairment in the industrialized world, currently impacting the elderly with a worldwide prevalence of 170 million individuals (28, 29). In particular, persistent complement dysregulation is associated with long-COVID (30), and alleles of complement factor H (CFH) and other complement genes represent major risk alleles for AMD (31–33). Any synergy between SARS-CoV-2 infection and AMD risk factors that accelerates the onset of AMD would have important public health consequences.

In this study, we show that SARS-CoV-2 and its major VOCs can reach and productively infect RPE cells in vivo, using two transgenic mouse models that express human ACE2 and mimic the human natural disease course. In addition, the virus also induced inflammatory responses in the retina, similar to those found in AMD (25, 27). Infection of RPE cell cultures resulted in altered RPE physiology and impaired functions. Using two independent lentiviral systems, we demonstrated the effect of Spike-mediated viral entry and viral proteins on RPE cells. Due to the key role of the RPE in supporting the photoreceptors, the significance of the RPE as a target for SARS-CoV-2 highlights an increased risk for potential long-term effects on vision arising from SARS-CoV-2 infection.

Results

SARS-CoV-2 can reach and infect RPE and induce local complement activation in a transgenic mouse model

To determine whether SARS-CoV-2 can reach and infect the RPE, following an intranasal inoculation, we conducted an in vivo infection using the reference strain 2019-nCoV/USA_WA1/2020 (hereafter referred to as WT) in two different mouse models that express human ACE2: Taconic AC70 mice and Jackson Laboratory K18 mice (Fig. 1A). Although the K18 mouse is the more widely used mouse model for SARS-CoV-2 infection, the AC70 mouse better replicates the ACE2 expression pattern in human retinal cells, many of which have been reported to express the ACE2 receptor (34, 35). Specifically, we found significant ACE2 expression in AC70 RPE (Figs. 1B and S1A), consistent with a previous report showing the RPE as one of the highest regions of ACE2 expression in the human eye (9). The mice received intranasal inoculation with 1×10^4 PFU WT virus (36), and their weight change was recorded (Fig. 1C). The mice were euthanized at 5 days post-infection (dpi) or 4 dpi if they met the humane endpoint sooner. All infected AC70 mice exhibited lethargy, gradual weight loss, and were immobile prior to euthanasia, while only two out of five infected K18 mice exhibited significant weight loss and milder symptoms. Upon euthanasia, we harvested one eye for immunofluorescence analysis, one for immuno-electron microscopy (EM) analysis, and the lungs for viral replication analysis via qRT-PCR (Fig. 1D). Details on the individual animals are summarized in Table S1.

By immunofluorescence of fixed eyecup flat mounts, using an anti-SARS-CoV-2 nucleocapsid (N) antibody (Fig. S1A), we did not detect any N-positive staining in the RPE of the infected K18 mice, and we detected positive staining in only two out of six infected AC70 mice euthanized at 4 dpi. However, all the AC70 mice that were euthanized later, at 5 dpi, contained clusters of positive staining cells throughout the RPE (Fig. 1E, Table S1). There was no relationship between lung viral titer and RPE infection (Table S1), so that a major factor for RPE infection appears to be the amount of time since inoculation.

To further assess viral infection in the RPE cells, we conducted immuno-EM with the same anti-SARS-CoV-2 N antibody. In immunogold-labeled positive RPE cells, we found gold particles throughout the RPE cell body (Fig. 1F), including the apical region and the microvilli (Fig. 1G). At higher magnification, we observed intact immunogold-labeled viral particles localized in the apical region of the mouse RPE (Fig. 1H).

Recent reports have shown an association between complement dysregulation and COVID severity, as well as an increased risk of long-COVID in patients (26, 30). Complement activation is also linked to impaired RPE health and AMD pathogenesis (31–33). Using immunofluorescence staining, we observed widespread, increased accumulation of complement components C3b and C5b-9 (MAC) across a region that appeared to include the basal RPE, Bruch's membrane, and choroid cells, in retinal sections of the SARS-CoV-2-infected AC70 mice, in contrast to the respective mock-infected animals (Fig. 1I, J). The widespread labeling of these complement components was evident even in areas where only a few cells showed productive infection by SARS-CoV-2, as indicated by SARS-CoV-2 N protein immunolabeling (Fig. 1J).

Together, these findings demonstrate that SARS-CoV-2 can infect the RPE and induce widespread complement activation across the RPE in mice expressing human ACE2.
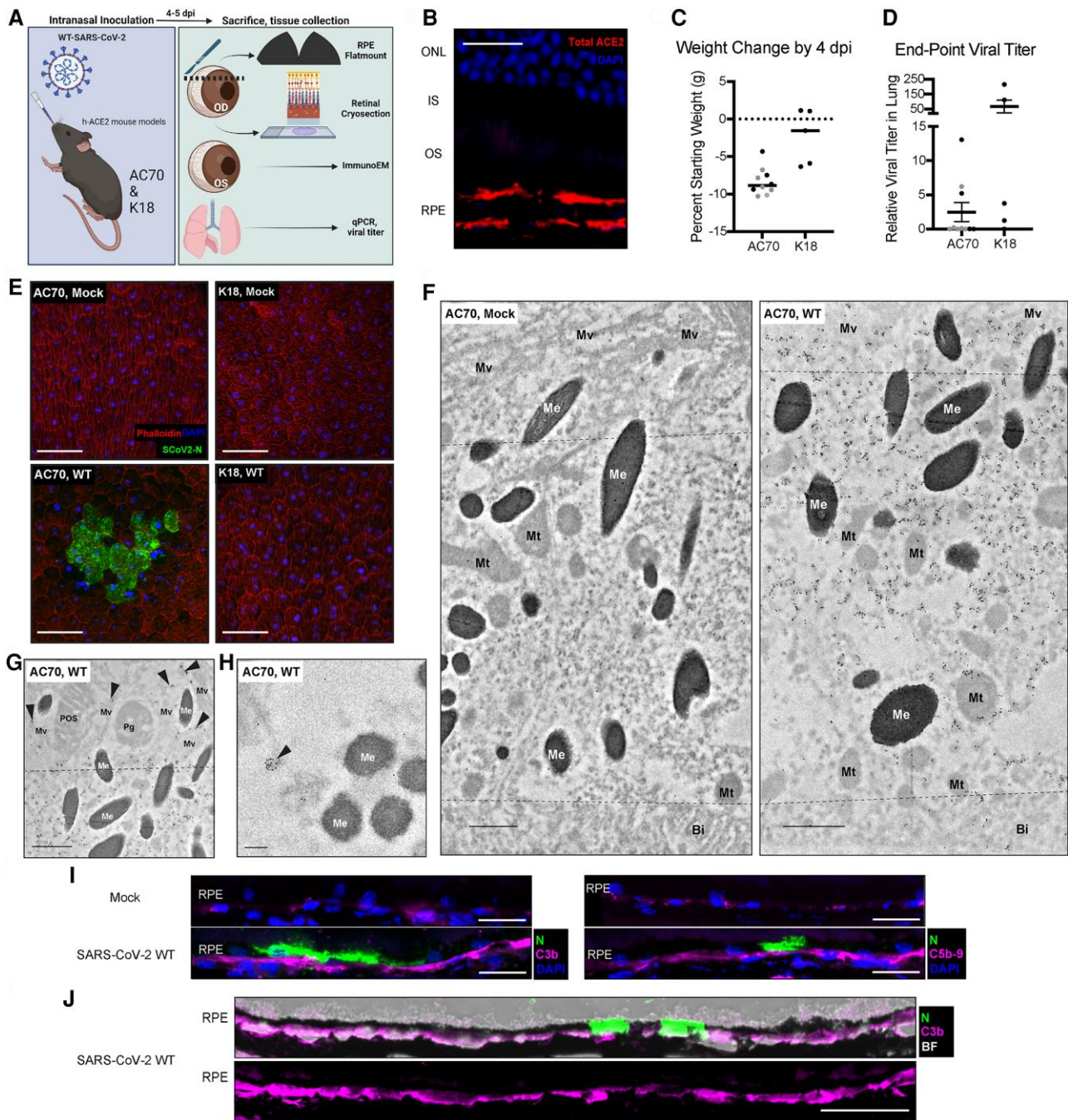
Fig. 1. SARS-CoV-2 can reach and infect the RPE in a transgenic mouse model. A) Intranasal inoculation of hACE2 mouse models. B) Immunofluorescence image of total ACE2 (mouse and human version) expression in retinal cryosections from the AC70 hACE2 transgenic mouse line. Scale bars: 20 μm. C) Percent weight change relative to starting weight of hACE2 mice infected with WT virus by 4 dpi. Each dot represents an individual mouse. The gray dots indicate mice sacrificed on day 4 due to severe disease, while the black dots indicate mice sacrificed on day 5. D) Relative viral replication in the lungs of hACE2 mice infected with WT virus, as measured by qRT-PCR. Each dot represents an individual mouse, as described in C. E) RPE flat mount from AC70 mice intranasally infected with mock or WT SARS-CoV-2 virus, showing immunofluorescence (green) of the SARS-CoV-2 N protein, as an indicator of viral presence. Scale bars: 50 μm. F–H) Immuno-EM labeling of SARS-CoV-2 N protein in the RPE of AC70 mice, intranasally infected with WT SARS-CoV-2 virus. Dotted lines indicate apical or basal region. Mv, microvilli; Me, melanosome; Mt, mitochondria; Bi, basal infoldings; POS; Pg, phagosome. F) Gold particles are evident throughout the RPE cell body of an infected mouse (but not a mock-infected mouse), indicating viral presence. G) Gold particles indicate viral presence in the apical region of the RPE, including the microvilli (black arrowheads). H) A cluster of gold particles indicate an intact viral particle (black arrowhead) inside an RPE cell. Scale bars: 2 μm (F, G), 200 nm (H). I) Retinal cryosections from AC70 mice intranasally infected with mock or WT SARS-CoV-2 virus, showing complement components C3b (left) and C5b-9 (right), labeled in magenta; SARS-CoV-2 N protein in green; and DAPI in blue. Scale bars: 20 μm. J) Lower magnification of a section through the RPE layer from an infected AC70 mouse: upper image, bright-field plus N protein (green) and C3b immunofluorescence (magenta); lower image, C3b immunofluorescence alone. Widespread accumulation of C3b is evident, despite only two small regions of N-protein expression. Scale bars: 50 μm.

SARS-CoV-2 can infect and replicate in human RPE cells

To test that SARS-CoV-2 can infect human RPE cells via endogenous receptors, we first confirmed whether human RPE cells express cell-entry receptors endogenously that are important for SARS-CoV-2 replication. We examined ACE2 and TMPRSS2 expression level in several human RPE cell models. Consistent with previous reports (14, 37), we found that both ACE2 and TMPRSS2 were expressed in all the human RPE cell models we tested at both RNA (Fig. 2A) and protein (Fig. 2B) levels. Using immunofluorescence staining and super-resolution microscopy, we found that ACE2 was localized mainly to the apical region of the RPE cells but was also found to a lesser extent on the basal–lateral surface (Fig. S1B).

We then tested in vitro whether SARS-CoV-2 infects human RPE cells. We investigated the response of the RPE to infections with the WT and major SARS-CoV-2 VOCs: B.1.617.2 (Delta) and BA.1 (Omicron). To visualize infection, we first incubated human ES-derived RPE (hES-RPE) cells grown on Trans-well filters with the SARS-CoV-2 WT strain tagged with mNeonGreen (WT-mNG) (38) for 1 h, and then fixed the cells at 48 h post-infection (hpi). We found that the RPE cells can be infected by the SARS-CoV-2 as indicated by the presence of the mNG+ cells (Fig. 2C). Infection was confirmed with immunofluorescence labeling for SARS-CoV-2 N (Fig. 2D) and Spike (S) (Fig. 2E) proteins. This labeling gave mostly consistent detection of SARS-CoV-2 compared with the mNG-tag (38), with an occasional difference in expression (Fig. S1C). Using transmission electron microscopy (TEM), we observed infected RPE cells 48 hpi with both intracellular vesicles filled with assembled viral particles, and viral particles attached to the apical surface of the cells, suggesting active viral production by infected RPE cells (Figs. 2F and S1D, E).

Next, we tested different factors that could affect SARS-CoV-2 infectability and viral production in RPE using the TCID$_{50}$ assay. First, by using 4-day-, 4-week-, and 10-week-old hES-RPE cells, we tested whether human RPE cultures of varying degrees of maturation impacted SARS-CoV-2 replication in vitro (39). We found that maximal viral production efficiency was similar regardless of culture age, as shown by TCID$_{50}$ in cell culture supernatants (Fig. 2G). Second, we tested whether newly produced SARS-CoV-2 virions were released apically as reported for upper airway epithelial cells (40), by comparing viral titer in the apical vs. the basal chambers of the Trans-well cultures. We tested both 4-day- and 4-week-old RPE cultures following an infection with the WT strain, using the TCID$_{50}$ assay. In both cases, we detected significantly higher viral titer in the apical chamber of the Trans-well than in the basal chamber, but the difference was larger in the more mature RPE cultures, possibly due to better developed barrier function (Fig. 2H). Third, we compared the infectability of SARS-CoV-2 variants mNG (WT), B.1.617.2 (Delta), and BA.1 (Omicron) in RPE cells. We found that all three variants can productively infect RPE cells. At 48 hpi, in cell culture supernatants of infected RPE cell cultures, Delta had a similar level of viral production to that of WT, whereas Omicron produced lower viral titers than WT and Delta (Fig. 2I). However, at 10 dpi, immunofluorescence detection of viral protein showed that Omicron viral production in the RPE cells is comparable to that of the WT (Fig. 2J). Finally, we performed time-course experiments with WT and Omicron to determine the duration of RPE cell infection. Time-course experiments showed that, although there were differences in viral titer with respect to the viral strain and the time post-infection, strikingly, a considerable amount of virus was still detectable 10 dpi with all three variants (Figs. 2K and S1F, G). Throughout the time course, we did not observe significant damage to the RPE monolayer (Fig. S1I).

Together, these results suggest that different SARS-CoV-2 VOCs can infect RPE cells, regardless of the maturity of the RPE cells (39). Furthermore, once infected, RPE cells sustain a high level of viral replication for as long as 10 days, with newly assembled viral particles released primarily from the apical surface of the RPE.

SARS-CoV-2 infection negatively impacts RPE morphology and physiology

To determine the effect of viral infection on RPE ultrastructure, we examined WT and Omicron-infected cells using TEM. We observed that many of the RPE cells infected with the WT virus were intact (Fig. 3A). Compared with the adjacent uninfected cells, the infected RPE cells had lost most of their apical microvilli. They also appeared swollen and extended further apically than uninfected cells (Fig. S2A). Remarkably, despite being inundated with fully assembled viral particles, the cell still possessed healthy-looking organelles, including melanosomes and cristae-dense mitochondria (Fig. 3A, inset). In contrast, many Omicron-infected RPE cells were damaged. From observations of cell remnants containing fully assembled viral particles, it appeared that the cells had undergone necrosis (Figs. 3B and S2B). Phalloidin staining showed that there was increased stress fiber formation in both WT and Omicron-infected RPE cells (Fig. 3C), as well as an apparent reduction in actin-rich apical microvilli (Fig. 3C, Y to Z panel), consistent with our TEM findings.

To tease apart the effects of different steps of the viral life cycle, we first tested the specific effect of Spike–ACE2-mediated viral entry on RPE by utilizing a Spike-pseudotyped lentivirus model (41). As indicated by red fluorescent protein (RFP) expression, human RPE cells could be infected by either the control VSVG-pseudotyped or the Spike-pseudotyped lentivirus (Fig. S2C, D). Unexpectedly, we noticed that the RFP expression pattern changed from diffuse, when infected with the control VSVG-pseudotyped lentivirus, to localization within specific cytoplasmic compartments, when cells were infected with the Spike-pseudotyped virus (Fig. S2C, D). These findings suggest potential changes in cell physiology induced by Spike-mediated viral entry. Moreover, a closer look at the Spike-pseudotyped virus-infected RPE cells revealed altered RPE morphology, including abnormal membrane protrusion/blebbing, increased presence of damaged cell debris, and basal deposits, when compared with cells infected with VSVG-pseudotyped virus (Figs. 3D and S2E).

Next, we sought to determine the effect of specific SARS-CoV-2 proteins on the RPE cells. The presence of high levels of viral proteins during viral replication and assembly can pose a huge burden on the host cell (42). Moreover, many SARS-CoV-2 proteins are found to interact with different parts of the host cells, interfering with their normal cellular and biological processes (43). Previous reports have shown that SARS-CoV-2 Envelope protein (E) and ORF3a protein (3a) are both involved in host-viral protein–protein interactions and are associated with cell immune responses (44). The E protein was shown to specifically interrupt epithelial cell junction stability (45), while 3a was shown to inhibit lysosomal function (46), two aspects of RPE cell biology that support essential functions of the RPE (21). To mimic SARS-CoV-2 viral replication, we used lentiviral-mediated expression of the E and 3a proteins and studied their effects on RPE morphology and physiology. We generated a pure population of cells stably expressing the E and 3a proteins by applying puromycin selection following lentiviral
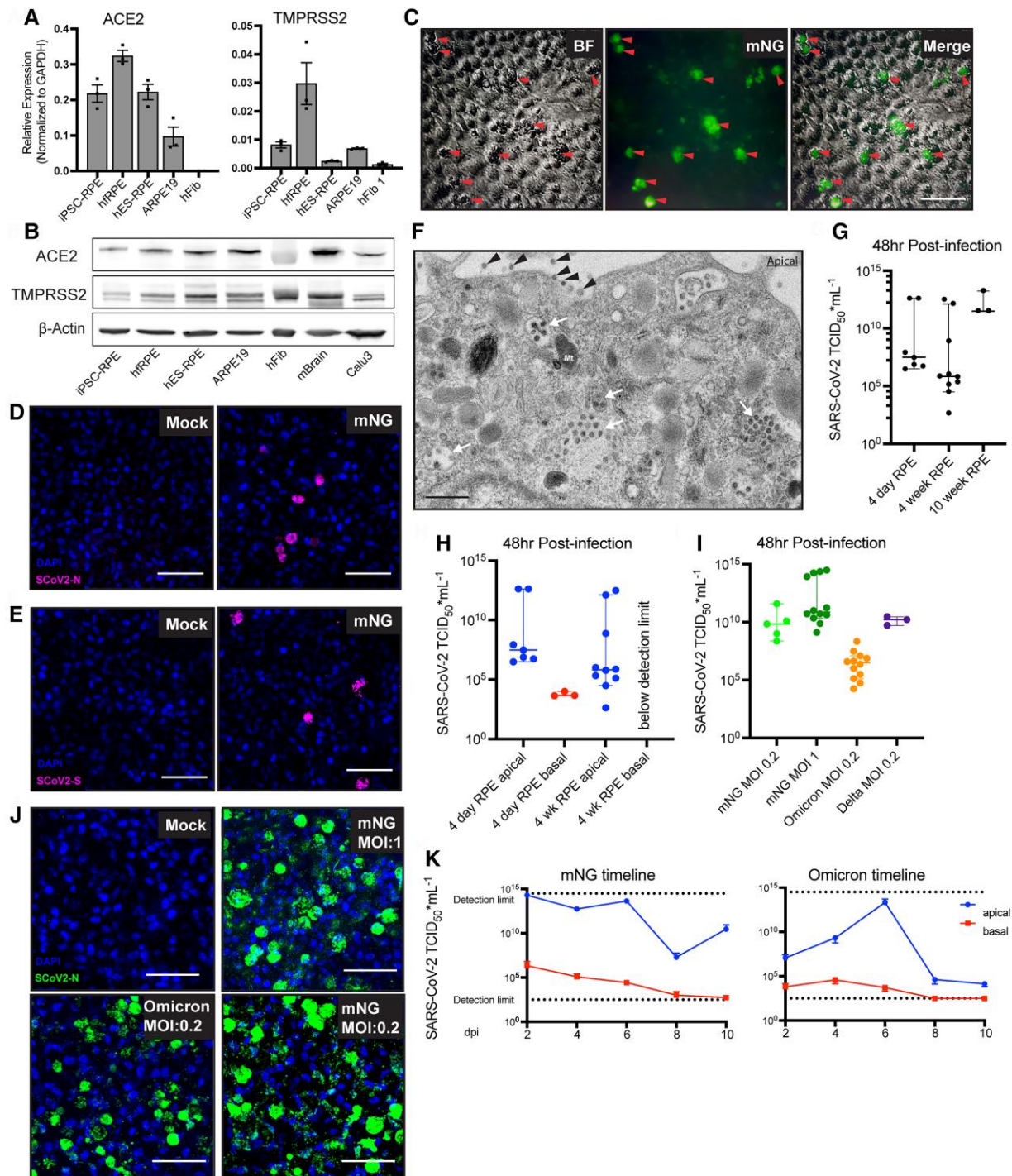
Fig. 2. SARS-CoV-2 can infect and replicate in human RPE cells. A) qPCR and B) western blot analysis for expression of major SARS-CoV-2 viral entry receptors, ACE2 and TMPRSS2, in different types of cells and tissues. Each dot in A represents a biological replicate. iPSC-RPE, human induced pluripotent stem cell-derived RPE; hfRPE, human fetal RPE; hES-RPE, human embryonic stem cell-derived RPE; ARPE-19, human RPE cell line; hFib, human fibroblasts; Calu3, human lung epithelial cell line; mBrain, mouse brain. C) Bright-field (left) and immunofluorescence (middle) image of hES-RPE cells infected by fluorescently tagged WT SARS-CoV-2 virus (MOI: 0.2), as indicated by mNeonGreen (mNG) signal. Scale bars: 50 µm. D–E) Immunofluorescence image of hES-RPE infected by WT SARS-CoV-2 virus (MOI: 0.2), as indicated by positive staining of SARS-CoV-2 N (D) and S (E) proteins. F) TEM analysis showing SARS-CoV-2 and infected hES-RPE in vitro with fully assembled viral particles. Black arrowheads indicate examples of individual viral particles on the apical surface of the RPE. White arrows indicate examples of intracellular compartments containing fully assembled viral particles. Mt, mitochondria. Scale bars: 2 µm. G) SARS-CoV-2-mNG viral replication and release by hES-RPE cells of different culture lengths 48 hpi (MOI: 1), measured by $TCID_{50}$ in Vero6 cells. H) Viral titer released by hES-RPE cells infected with WT SARS-CoV-2 virus in the apical vs. basal chamber of the Trans-well cultures, 48 hpi. Each dot represents an individual culture. I) Average viral production of mNG (WT), Omicron, and Delta by hfRPE cells 48 hpi. Each dot represents an individual culture. J) Immunofluorescence images of hfRPE cells 10 dpi with mock (top left panel), mNG (MOI: 1, top right panel, MOI: 0.2, bottom right panel), and Omicron (MOI: 0.2, bottom right panel), stained with antibodies against SARS-CoV-2 N and S proteins, both labeled in green. Scale bars: 50 µm. K) Representative viral production kinetics of mNG (WT) and Omicron in the apical vs. basal chamber of the Trans-well culture over time. Dotted line signifies the upper and lower detection limit of the assay. G–I) Graph shows median with 95% CI.
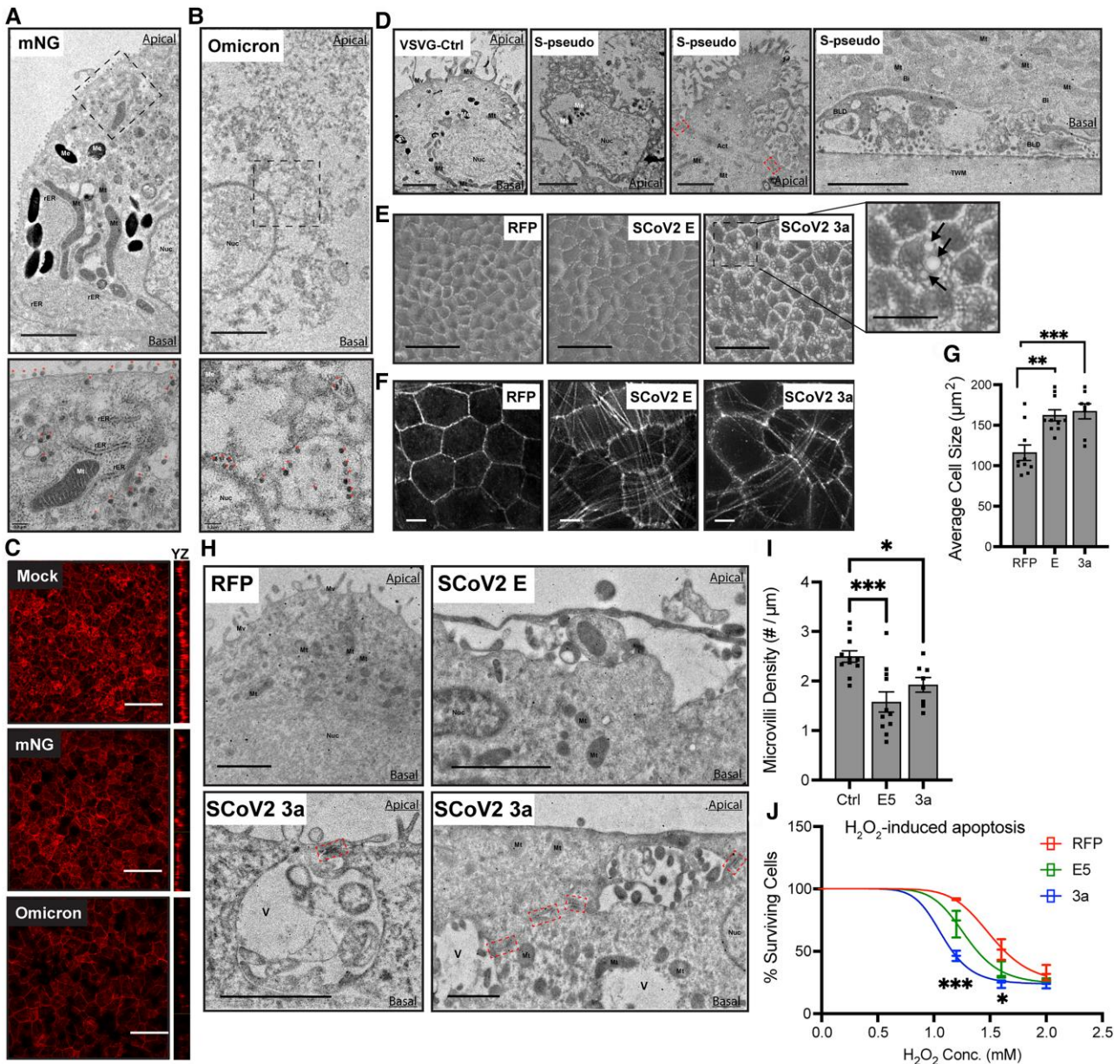
Fig. 3. SARS-CoV-2 infection alters RPE morphology and negatively impacts RPE physiology. Representative TEM images of hfRPE cells infected with mNG (WT) (A) and Omicron (B) variants. Boxed areas are magnified below; small red asterisks indicate viral particles. Mv, microvilli; Me, melanosome; Mt, mitochondria; Nuc, nucleus; rER, rough endoplasmic reticulum. Scale bars: 2 μm (upper) and 200 nm (lower). C) Projected fluorescence images of hfRPE cells infected with mNG (WT) or Omicron showing decreased phalloidin staining (red) of apical f-actin, indicating less extensive apical microvilli in Omicron-infected cells. Right panels show phalloidin staining of apical microvilli in mock and infected RPE monolayers in the Y–Z plane. Scale bars: 50 μm. D) Representative TEM images of iPSC-RPE cells exhibiting perturbed RPE morphology 2 weeks after infection by Spike-pseudovirus. Act, actin; Bi, basal infoldings; BLD, basal laminar deposit; TWM, Trans-well membrane. Red boxes indicate remnants of tight junctions between adjacent cells. Scale bars: 2 μm. E) Representative bright-field images of differentiated ARPE-19 cells, expressing control RFP or SARS-CoV-2 E and 3a proteins. Arrows indicate vacuole-like structures. Scale bars: 50 and 20 μm for the magnified panel. F) Representative phalloidin staining of ARPE-19 cells expressing control RFP or SARS-CoV-2 E and 3a proteins showing an increased presence of stress fiber in cells expressing SARS-CoV-2 proteins. Scale bars: 5 μm. G) Average size of ARPE-19 cells expressing RFP (control) vs. SARS-CoV-2 E and 3a proteins. Each dot represents an individual culture. H) Representative TEM images of ARPE-19 cells, expressing either control RFP or SARS-CoV-2 E or 3a protein. Mv, microvilli; Mt, mitochondria; Nuc, nucleus; V, inter- or intracellular vacuole. Red boxes indicate remnants of tight junctions between adjacent cells. Scale bars: 2 μm. I) Average microvillus density in ARPE-19 cells expressing control RFP, SARS-CoV-2 E and 3a proteins, as identified in TEM images. J) Survival curves of ARPE-19 cells expressing control RFP or SARS-CoV-2 E or 3a protein, following H_2O_2 treatment. Average results of three separate experiments. G), I) Data represent mean ± SEM. J) Plot shows mean with minimum and maximum value. One-way ANOVA with multiple comparison test. $^*P < 0.05$, $^{**}P < 0.01$, $^{***}P < 0.005$.

transduction. Expression of both viral proteins was confirmed by RNA (Fig. S2F) and protein (Fig. S2G) analysis. For microscopy analysis, the E- and 3a-expressing cells, as well as control cells expressing an RFP construct, were seeded on Trans-well filters and cultured for 4–6 weeks in nicotinamide-supplemented growth media to promote the formation of fully differentiated, confluent monolayers (47, 48). Under low-magnification bright-field microscopy, the only clear difference among the three lines was apparent vacuolization of some but not all 3a-expressing cells (Fig. 3E); vacuolization was also, but only rarely observed in some cultures
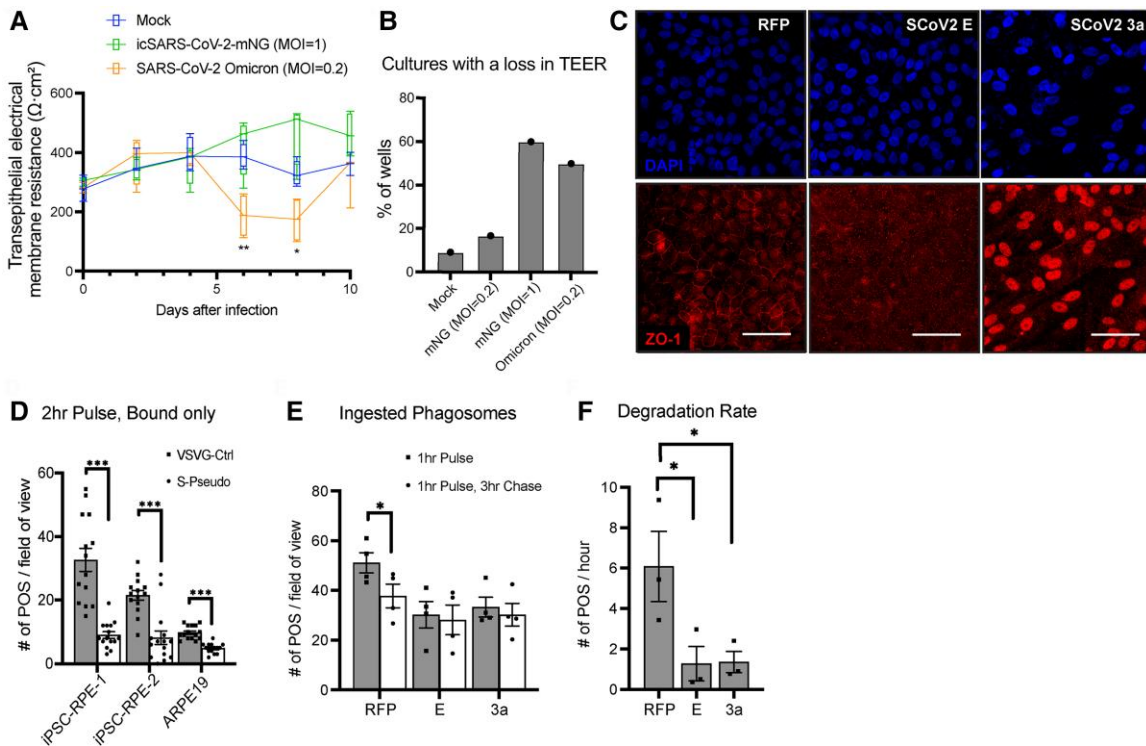
Fig. 4. Effect of SARS-CoV-2 infection on RPE barrier function and phagocytic capacity. A) Representative average TEER measurements of 4-week-old hfRPE culture over 10 dpi of mock, mNG (WT, MOI: 1), and Omicron (MOI: 0.2). Box and whisker graph shows mean with minimum and maximum values. B) Percentage of cultures for each condition that showed a decrease in TEER values (i.e. lower than the preinfection value on day 0) within 10 dpi. C) Representative fluorescence images of ARPE-19 cells expressing SARS-CoV-2 E and 3a proteins showing a reduction in ZO-1 junctional expression. Scale bars: 50 μm. D) In vitro phagocytosis assay in iPSC-RPE and polarized ARPE-19 cells infected with VSVG-Control and Spike-pseudotyped lentivirus, showing reduced phagosome binding following Spike–ACE2-mediated viral entry. E) Number of ingested POS phagosomes following a pulse-chase experiment of in vitro phagocytosis assay, identified by inside–outside immunofluorescence labeling of rod photoreceptor opsin in ARPE-19 cells expressing control RFP, SARS-CoV-2 E, and 3a proteins. F) Rate of POS phagosome degradation during the 3-h chase in the in vitro phagocytosis assay in ARPE-19 cells expressing control RFP, SARS-CoV-2 E, and 3a proteins. D–F) Each dot represents an individual culture. Graph shows mean ± SEM. D, E) Unpaired equal-variance Student's t test. A, F) One-way ANOVA with multiple comparison test. $^*P < 0.05$, $^{**}P < 0.01$, $^{***}P < 0.005$.

of E-expressing cells. However, when stained with phalloidin, only the control cells showed the characteristic f-actin organization of a well-differentiated epithelial cell; some of both the E- and 3a-expressing cells possessed actin stress fibers (Fig. 3F). In addition, the E- and 3a-expressing cells exhibited a somewhat larger surface area relative to the control cells (Fig. 3G), characteristic of a distressed RPE layer (49). TEM analysis revealed markers of cellular stress, such as condensed chromatin, membrane blebbing, and the presence of inter- and intracellular vacuoles in E- and 3a-expressing cells (Figs. 3H and S2H). In addition, the apical microvilli in both E- and 3a-expressing cells were reduced (Fig. 3H, I).

A potential explanation for these observations is that the presence of viral proteins led to reduced RPE cell viability, which could result from changes in the cell proliferation rate. To test this hypothesis, we plated the cells at low density and evaluated their proliferation rate over 72 h using an XTT assay. However, we did not observe consistent changes in proliferation rate between control and viral protein-expressing cells (Fig. S2I).

SARS-CoV-2 3a is known to induce oxidative stress and cell death in some mammalian cell types (50, 51). Therefore, we checked to see whether the expression of viral proteins increased RPE sensitivity to oxidative stress–induced cell death. We plated cells at confluency and exposed them to increasing concentrations of H_2O_2. Using an XTT assay again, we found that, although there was no decrease in cell viability between the control and viral protein-expressing cells in the absence of H_2O_2, we observed a greater sensitivity to

H_2O_2-induced cell death in both E- and 3a-expressing cells compared with the control cells (Fig. 3J). Overall, our findings suggest that SARS-CoV-2, through ACE2-mediated viral entry and the production of toxic viral proteins such as ORF3a, negatively impacts RPE cells by causing morphological changes and increased RPE sensitivity to oxidative stress.

SARS-CoV-2 infection impairs RPE barrier function and phagocytic capacity

Located between the photoreceptors and the choroidal capillaries, the RPE performs many important functions to maintain the health and function of the outer retina (21, 22). Given the cellular damage caused by SARS-CoV-2 in RPE cells (Fig. 3), we hypothesized that SARS-CoV-2 infection would significantly interfere with RPE functions. One such function is regulating material exchange between the photoreceptors and the choroidal vessels by forming the outer blood–retina barrier. To test whether SARS-CoV-2 infection interferes with RPE barrier function, we measured the transepithelial electrical resistance (TEER) over time in mock-infected cells and those infected with different SARS-CoV-2 variants. We observed a transient yet significant reduction in RPE barrier function following Omicron infection (Fig. 4A). This reduction in TEER coincided with peak viral production, at 6 dpi (Fig. 1H). We also observed an increased incidence of the TEER value falling below that of day 0 (preinfection), following infections of all the strains (Figs. 4B and S4), including Delta (three out of three cultures tested). Consistent
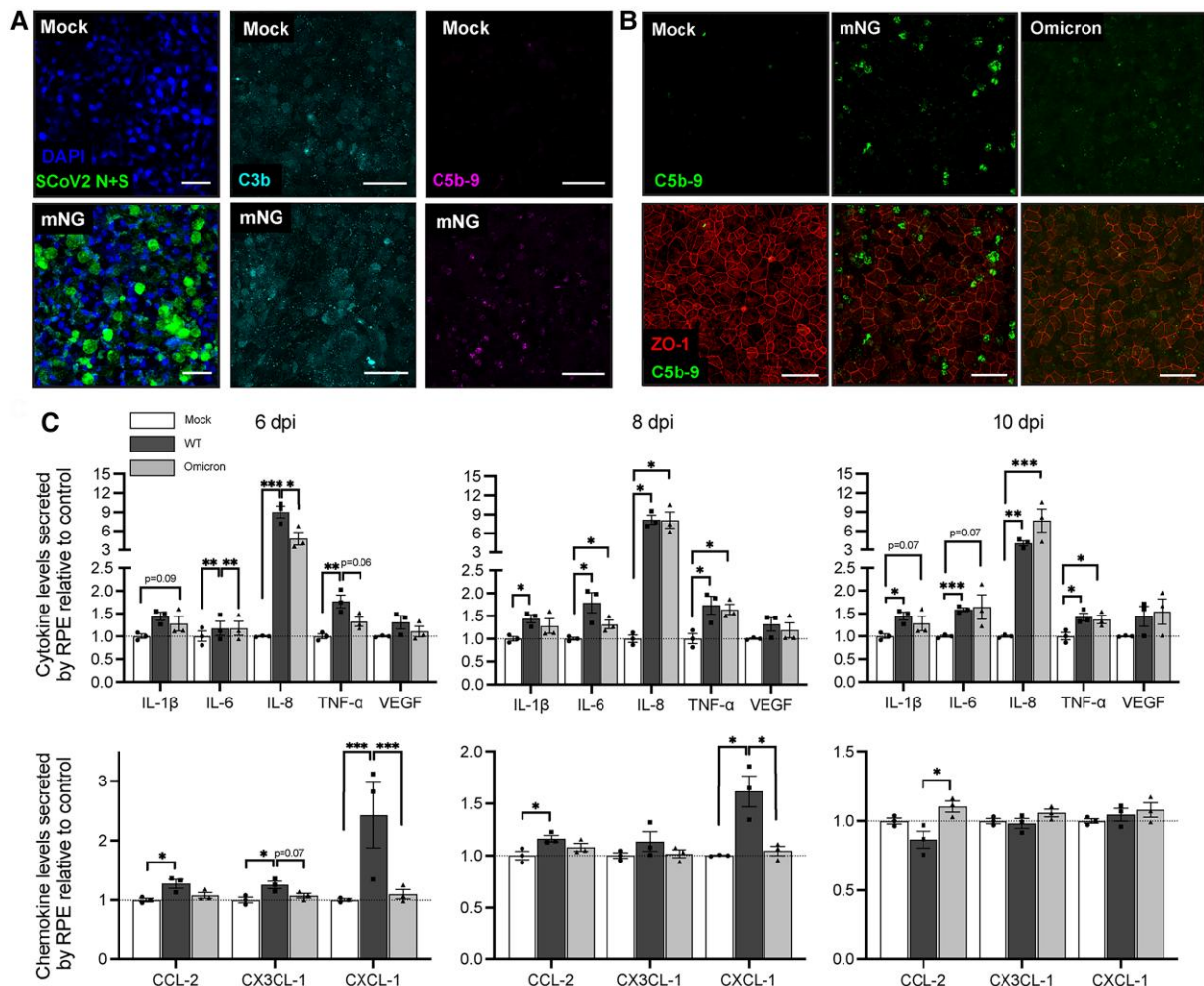
Fig. 5. SARS-CoV-2 infection causes an inflammatory response in RPE cells. A) Representative images of SARS-CoV-2 mNG (WT, MOI: 1)-infected hfRPE cells. Infection was detected by immunofluorescence labeling of SARS-CoV-2 N and S proteins, both labeled in green (left panel). Increased complement activation in infected cells is evident by increased immunofluorescence labeling of complement components, C3b (middle panel) and C5b-9 (right panel), 48 hpi. Scale bars: 50 μm. B) Representative images of hfRPE cells infected with mNG (WT) and Omicron 10 dpi. Immunofluorescence labeling showing decreased ZO-1 expression (red), but increased C5b-9 level (green) compared with the mock-infected cells. Scale bars: 50 μm. C) Cytokine and chemokine production was determined by multiplex Luminex immunoassays in cell culture supernatants of mock- and SARS-COV-2-infected RPE cells at 6, 8, and 10 dpi, with either WT or Omicron variant. Data graphed are normalized to mock-infected cells. Each dot represents an individual culture and the average of at least two technical replicates. Data represent mean ± SEM. Unpaired equal-variance Student's t test was conducted. *$P < 0.05$, **$P < 0.01$, ***$P < 0.005$.

with the loss of TEER value, we also found a reduction in the immunofluorescence labeling of the tight junction protein, ZO-1, in both WT and Omicron-infected cells (Fig. 5B). Interestingly, the presence of each of the SARS-CoV-2 proteins, E and 3a, alone, had a large effect on ZO-1 localization (Fig. 4C).

Another important function of the RPE is the regular ingestion of photoreceptor outer segment (POS) tips, which is followed by intracellular trafficking and endolysosomal digestion of the resulting phagosome. Using an in vitro phagocytosis assay (52) and the Spike-pseudotyped lentiviral system, we first investigated the effect of Spike-mediated viral entry on RPE phagocytosis of POS. To identify only the extracellularly bound POS, following a short-pulse feeding, we labeled with RHO antibodies without permeabilizing the cells. Compared with the cells infected with VSVG-Control lentivirus, those infected with Spike-pseudotyped lentivirus had significantly fewer bound POS (Fig. 4D).

POS binding to RPE is mediated by αvβ5 integrin (53). Interestingly, integrins were proposed to be potential co-receptors for SARS-CoV-2 viral entry. According to an in silico meta-analysis,

αvβ5 and αvβ3 are the two integrins most likely responsible for SARS-CoV-2 Spike protein binding and there was significant sequence homology between part of the Spike protein receptor-binding domain and the binding sequence commonly recognized by the integrin extracellular domains (54, 55). Therefore, we sought to determine whether the reduced POS binding is due to the involvement of αvβ5 in Spike-mediated viral entry into the RPE. Using immunofluorescence labeling, we observed reduced αvβ5 expression by RPE cells following S-pseudo virus infection, compared with VSVG-Ctrl virus infection (Fig. S3A). This was also observed in RPE cells infected with the SARS-CoV-2 (Fig. S3B). To further test the role of αvβ5 in Spike-mediated viral entry, we performed functional blocking of αvβ5 using a monoclonal antibody against a composite epitope on the αvβ5 native heterodimer integrin (56). We did not observe any difference in cells infected with the VSVG-Ctrl virus, whether or not they were pretreated with the blocking antibody. However, we saw a significant reduction in RFP signal in RPE infected with the S-pseudo virus, following blocking antibody treatment, compared with cells that were not treated (Fig. S3C).

Together, these data add to the recent reports demonstrating the importance of integrin activation in SARS-CoV-2 viral entry and pathology in different cell types (57–59).

It has been reported that SARS-CoV-2 hijacks the endolysosomal pathway of the host cells for many steps of its life cycle (60). Since the endolysosomal pathway is also critical to the digestion of the POS phagosomes (21), we tested whether the presence of SARS-CoV-2 proteins affected the phagosome degradative capacity of RPE cells. We conducted an in vitro phagocytosis pulse-chase assay in the control and viral protein-expressing cells, followed by inside vs. outside labeling, using an antibody against rhodopsin to identify ingested phagosomes containing POS membranes (61). Comparing the pulse-only with pulse-chase cells, we only saw a significant decrease in ingested phagosome number in the RFP control cells, but not the ones expressing SARS-CoV-2 proteins (Fig. 4E). This translates into a significant reduction in the degradation rate of POS phagosomes (Fig. 4F), suggesting that the presence of viral proteins delayed phagosome degradation. Collectively, our data demonstrate that SARS-CoV-2 infection of RPE cells directly impairs their barrier function and phagocytic capacity of POS by affecting αvβ5 integrins.

SARS-CoV-2 infection activates a prolonged inflammatory response in RPE

Acute and secondary inflammation following SARS-CoV-2 infection has been associated with many COVID-19-related pathologies, including long-term neurological symptoms (4, 25). Within the visual system, the RPE is a major regulator of the inflammatory response in the retina, which is an important factor in many retinal degenerations, including AMD (62, 63). To test whether SARS-CoV-2 infection in the RPE elicits an inflammatory response, we examined complement activation as well as cytokine and chemokine secretion by RPE cells.

Consistent with our in vivo findings, we observed increased complement activation in the hRPE cultures infected with WT virus, as indicated by elevated expression of C3b and the membrane attack complex (C5b-9 or MAC) at 48 hpi (Fig. 5A). Increased levels of C5b-9 (MAC) were also observed at 10 dpi, although they were higher in cells infected with WT virus than with Omicron (Fig. 5B). Interestingly, using the Spike-pseudotyped lentiviral model, Spike-mediated viral entry alone also elicited complement activation in the RPE cells, along with downregulation of the ACE2 receptor (Fig. S5A).

The RPE is also known to contribute to the unique immune status of the retina by secreting a variety of antiinflammatory as well as proinflammatory cytokines and chemokines (63), some of which are also associated with poor prognosis in AMD (27). Using the Luminex multiplex cytokine array, we investigated the secretion kinetics of various cytokines and chemokines in a time-course experiment following a single 1-h infection (Fig. 5C). We found that infection with WT SARS-CoV-2 resulted in higher secretion of proinflammatory cytokines such as IL-1β, IL-6, IL-8, and TNF-α into the apical chamber of RPE cells at 6, 8, and 10 dpi compared with uninfected RPE cells. Infection with the Omicron variant induced secretion of IL-6 and IL-8 by RPE cells at 8 dpi and of TNF-α at 6, 8, and 10 dpi compared with uninfected RPE cells. Infection with WT SARS-CoV-2 also led to higher secretion of proinflammatory chemokines such as CX3CL1 and CXCL1 into the apical chamber of RPE cells at 6 dpi compared with uninfected RPE cells, while consistent upregulation was not observed at 8 and 10 dpi. Neither WT nor Omicron SARS-CoV-2 affected the secretion of CCL2 and VEGF by RPE cells. Unlike WT

SARS-CoV-2, Omicron SARS-CoV-2 also had no effect on the secretion of IL-1β, CX3CL1, and CXCL1 by RPE cells at any time point. Infection of RPE cells with a similar amount of SARS-CoV-2 (MOI: 0.2) induced different proinflammatory signatures between the WT and Omicron SARS-COV-2 variants in RPE cells; overall Omicron SARS-CoV-2 induced a less prominent and more delayed inflammatory response in RPE cells than WT SARS-CoV-2 did.

In summary, SARS-CoV-2 infection appears to induce a proinflammatory response in the RPE cells that involves complement activation and increased production and secretion of inflammatory cytokines. Moreover, specific differences in this response between the WT and Omicron SARS-COV-2 variants were observed.

Discussion

In the present study, we showed that SARS-CoV-2 can reach and infect the RPE through its apical surface in transgenic mice that express human ACE2; entry is most likely via ACE2 and αvβ5. To address the consequences of infection on the human RPE, we investigated infection of human RPE cultures by major VOCs of SARS-CoV-2. Using independent lentiviral systems, we found that the SARS-CoV-2 Spike (S)-mediated viral entry alone, and the presence of viral Envelope (E) and ORF3a (3a) proteins can induce morphological changes and physiological damage to the RPE cells. Infection with both the original strain (WT) and the Omicron subvariant caused complement activation as well as the production of cytokines and chemokines, including IL-1β, IL-6, IL-8, and TNF-α. As a consequence of in vivo infection, the RPE cell layer showed widespread complement activation, even when only some RPE cells showed productive infection.

Route of SARS-CoV-2 to the RPE

Consistent with previous reports (14), we detected ACE2 and TMPRSS2 expression in all human RPE cell culture types tested, with ACE2 expressed primarily on the apical surface of the RPE, and a minor portion on the basal–lateral membrane. Indeed, most retinal cell types are known to express the viral entry factors, ACE2 and TMPRSS2 (34, 35), supporting a plausible route of infection from the inner retina. We also identified RPE apical-specific integrin αvβ5 (53) as a possible co-receptor for viral entry, similar to its role in internalizing adenovirus (64, 65) and Zika virus (66). Together, these data suggest that RPE infection primarily occurs through its apical surface via interactions between the viral S protein and host integrins, ACE2 and TMPRSS2.

Interestingly, with two of the most used hACE2 mouse models to study SARS-CoV-2 infection, we observed RPE infection only in the AC70 mice, but not in the K18 mice. This observation could be due to a difference between the two mouse lines with respect to the cell types expressing hACE2, or, more specifically, with respect to hACE2 expression levels in the brain and vascular endothelial cells (67). Since we observed RPE infection in mice infected intranasally, the virus likely reached the RPE apical surface either through viremia (16) or infected immune cells migrating from the inner retinal vasculature, or antero/retrograde transmission from the optic nerve following CNS infection (68, 69). The neuronal route is strongly supported by a recent publication demonstrating limited systemic infection in the AC70 mouse model (70). While we cannot rule out the chance of grooming behaviors causing infection through the corneal surface (71, 72) in the intranasally infected mice, the absence of ocular infection in the K18 mice in our study and the debatable accessibility of the corneal epithelium (73, 74) suggest that this is an improbable route. A

provocative alternative hypothesis is that a gut–retina barrier breach due to the CRB1 mutation harbored by the AC70 mice (75) might have contributed to increased RPE susceptibility to viral invasion.

Interestingly, we found no direct relationship between lung viral titer and RPE infection (Table S1), suggesting that ocular infection can occur regardless of the severity of the systemic disease. Moreover, the infected animals that had no detectable RPE infection were all sacrificed on 4 dpi, while the infected AC70 mice sacrificed on 5 dpi all showed productive infection in the RPE, suggesting that a major factor for RPE infection is the time it takes for the virus to travel to the RPE. Supporting this suggestion, a recent study (20) reported detected SARS-CoV-2 in the retinas of K18 mice 7–21 days after intranasal inoculation with 4×10^2 PFU of virus. This viral titer was 25 times lower than that used by us, resulting in longer survival times, and thus allowing examination at a longer interval after inoculation. Together, these data suggest that ocular infection can occur regardless of viral dosage or severity of the systemic disease.

SARS-CoV-2 variants

We directly assessed differences among infections of the WT strain and two major SARS-CoV-2 VOCs, Delta and Omicron. All three strains readily infected and replicated in the RPE cells for an extended period, albeit with slightly different kinetics. We measured an overall lower viral titer with Omicron infection than with either WT or Delta infections. This is possibly due to cell loss from the cultures due to the increased cell death we observed following Omicron infection. Alternatively, this may arise from the interaction between host and viral proteins, resulting in a cell type–specific effect on viral growth and genetic stability (76). All three strains caused a transient reduction in RPE barrier function, and similar types of cytokine and chemokine production. However, Omicron infection appeared to have different cytokine production kinetics than the WT virus with a latent but strong and prolonged production of both IL-6 and IL-8. This result points to the possibility that although Omicron might only cause mild disease in lung tissues, it could be more severe with regard to the long-term impact on organs such as the eye.

Effect of SARS-CoV-2 infection on RPE morphology

SARS-CoV-2 infection caused changes in RPE cell morphology. One such change, which could be seen in low-magnification bright-field images, is that the infected cells often protruded out of the monolayer with an irregular appearance compared with the adjacent noninfected cells. This effect could have been caused by overall cell swelling or the apical accumulation of prerelease vacuoles containing viral particles. Alternatively, it could have been caused by specific viral proteins. The presence of SARS-CoV-2 3a protein also led to the appearance of intra- or intercellular vacuoles. These vacuoles could be linked to the role of the 3a protein in promoting viral release via lysosomal exocytosis as a viroporin or its interaction with host proteins such as ZO-1 (46, 50, 77, 78). Another observed change was the striking loss of apical microvilli in SARS-CoV-2-infected RPE cells and cells expressing viral proteins E and 3a. This loss could be due to a general decline of cell physiology and structure, or a specific effect of proteins E and 3a on a polarization-related pathway. These morphological changes were not apparent in the in vivo model, likely due to the short-term exposure of the in vivo experiment.

Effect of infection on RPE function

Studies have shown that SARS-CoV-2 E and 3a proteins interact with host junctional proteins (79–81), and thus interfere with epithelial cell polarity (77, 78). This effect is further confirmed in our study with RPE cells, infected by SARS-CoV-2 or simply expressing SARS-CoV-2 E and 3a: ZO-1 had lower expression and was mislocalized, and, in some cases, actin stress fibers became evident. We also observed a transient reduction of TEER in RPE cells infected with different SARS-CoV-2 variants, suggesting compromised RPE barrier function. Loss of RPE junction integrity and increased permeability have been associated with retinal edema (82). Therefore, these findings could explain the occurrence of macular edema, the most common acute ocular manifestation that affects vision in patients with COVID-19 (83).

Another important role of RPE is its regular ingestion of POS tips. Defects in any stage of this multistep process can lead to RPE and photoreceptor damage and retinal degeneration (84). Here, we identified αvβ5, the integrin that is required for POS binding to initiate phagocytosis, as a potential viral entry co-receptor in the RPE (53). The Spike–integrin-mediated viral entry leads to a significant reduction in POS binding. This effect could result from altered surface availability of αvβ5, following binding and activation by the Spike protein (59). Consistent with this hypothesis, we observed a reduction in αvβ5 expression in the RPE following pseudovirus infection. In addition, we found that the presence of SARS-CoV-2 proteins E and 3a also impairs POS phagosome degradation. This effect might result from a general decline of cellular health and function from mitochondrial dysfunction, oxidative stress, ER stress, and inflammation caused by these viral proteins (50, 85, 86). Alternatively, it could be due to direct interference of these proteins with lysosomal pH and function. SARS-CoV-2 E protein can increase the pH of intracellular organelles such as lysosomes and ER-GIC, owing to its viroporin function (87). SARS-CoV-2 3a protein has also been identified as a viroporin (44, 50), but, in addition, it can also interfere directly with and hijack the endolysosomal pathway to facilitate viral reproduction and release (50). As the last step in RPE phagocytosis of POS (21), defective lysosomal function can cause abnormal accumulation of POS phagosome material and RPE pathology underlying some retinal degenerations (22, 88–90). Further studies are required to elucidate the specific roles of individual viral proteins and their interaction with host proteins. Together, these data demonstrate that SARS-CoV-2 infection impairs RPE function and could have a lasting effect on photoreceptor and retina health.

Inflammatory response and comparison with AMD

Acute and secondary inflammation following SARS-CoV-2 infection has been associated with many COVID-19-related pathologies, including those with long-term neurological impact (25). Our data demonstrate that SARS-CoV-2 infection in RPE also leads to complement activation and the production of numerous cytokines, including TNF-α, IL-1β, IL-6, and IL-8. These responses are remarkably similar to those during retinal pathologies such as AMD (27) and are consistent with the role of the RPE as the major regulator of the retinal immune response (22, 62, 63, 91). In addition, we found that, regardless of lung viral titer, increased accumulation of complement components in the outer retina was observed only in animals with RPE infection, implicating a local complement response. Moreover, the complement activation was not limited to the infected cells, but was widespread across

the RPE cell layer, most likely due to the secretion of proinflammatory cytokines to the extracellular space (26, 92, 93). Complement hyperactivation and dysregulation have been associated with COVID-19 severity (26, 30); single-nucleotide polymorphisms of various complement pathway components, including CFH, appear to be risk factors for COVID morbidity and death (93). Importantly, the persistence of increased complement activation has been linked to increased risk of long-COVID (26, 30).

Dysregulated complement activation and mutations, especially in the CFH gene (31–33), but also other complement genes (e.g. C3, BF/C2, and CFI) (94–96), are also major risk factors for AMD, which is the main cause of visual impairment in the industrialized world (28, 29). Our in vivo and in vitro findings on the inflammatory response of the RPE to SARS-CoV-2 infection, combined with reports of prolonged dysregulation of complement in long-COVID (26, 30), therefore suggest that SARS-CoV-2 infection could accelerate the onset and progression of AMD. Interestingly, HIV infection has been associated with a significant increase in the prevalence of AMD, especially at younger ages, with the suggested involvement of activation of the innate immune system (97–99).

AMD typically first affects the rod-rich region of the macula, by shortening the rod POSs. This initial effect results in relatively mild symptoms, such as decreased retinal sensitivity, delayed dark adaptation, and reduced contrast sensitivity. As the disease progresses more centrally in the macula, the cone photoreceptors in the center of the macula (the fovea) become damaged, and a patient's vision is impacted severely as visual acuity declines (100–104). Severe visual impairment from AMD thus takes a while to develop and is typically found only among the elderly. However, an earlier onset of AMD would increase the number of younger people with impaired vision, and, if due to an effector as widespread as SARS-CoV-2 infection, it would have significant implications for public health.

Materials and methods

All experimentation, including in vivo SARS-CoV-2 infection experiments in BSL3 facilities at the University of Southern California (USC) and UCLA, was approved and conducted in compliance with IACUC and biosafety regulations: USC IACUC protocol 21274, IBC protocol APPL-21-00081; UCLA IACUC protocol ARC-2021-012 (O.S.S.), IBC protocols BUA-2018-088-012-CR (D.S.W.) and BUA-2019-092-003-A (O.S.S.). Experimental details are given in the Supplementary Information. Briefly, SARS-CoV-2 viral stocks originated from the Biodefense and Emerging Infectious Disease Unit at the National Institute of Allergy and Infectious Disease (BEI-NIAID) were: (i) isolate USA-WA1/2020 (WT), (ii) isolate hCoV-19/USA/MD-HP05285/2021 (Lineage B.1.617.2; Delta Strain), NR-55671, provided by Andrew S. Pekosz; and (iii) isolate hCoV-19/USA/GA-EHC-2811C/2021 (Lineage B.1.1.529; Omicron Strain), NR-56481, provided by Mehul Suthar. The fluorescently tagged WT SARS-CoV-2 (icSARS-CoV-2-mNG; WT-mNG) was from Pei-Yong Shi's lab at the University of Texas Medical Branch. All SARS-CoV-2 strains were propagated in Vero-E6 or Vero-E6-TMPRSS2-hACE2 (Vero-T2A) cells. Viral titers were determined by assessing cytopathic effect in median tissue culture infectious dose (TCID50) assays in Vero-T2A cells. For the in vivo experiment, 8–10-week-old K18-hACE2 C57BL/6 (Jackson Laboratories) and AC70 (Taconic) mice were infected with 1×10^4 PFU of WT SARS-CoV-2 intranasally and monitored daily.

Acknowledgments

Supplementary Material

Supplementary material is available at PNAS Nexus online.

Funding

Author Contributions

N.W.H., A.P., T.K., O.S.S., and D.S.W. were involved in conception and design of experiments and analysis and interpretation of data and wrote the manuscript. N.W.H. performed functional, structural, and biochemical analysis of in vitro human RPE models. N.W.H. and S.T. processed and analyzed the in vivo infection experiment samples. A.P. and J.N. were involved in all BSL3 work connected to live SARS-CoV-2 in vitro infection. C.O. performed mouse lung viral replication qRT-PCR assays. M.S. and T.K. performed immunoassays. T.Z. performed EM sample preparation and some image analysis. B.L.B. performed XTT cell viability assays. S.T., R.K., and B.S. performed confocal microscopy sample preparation and analysis. All authors read and approved the final manuscript.

Data Availability

All values underlying graphed data and reported means presented in both the main text and supplemental material are provided in the Supporting Data Values file. All relevant data and materials related to this study are included in the manuscript and the supporting information.

References

1. Koff WC, et al. 2021. Development and deployment of COVID-19 vaccines for those most vulnerable. Sci Transl Med. 13:eabd1525.

2. Christie MJ, et al. 2021. Of bats and men: immunomodulatory treatment options for COVID-19 guided by the immunopathology of SARS-CoV-2 infection. Sci Immunol. 6:eabd0205.

3. Nyberg T, et al. 2022. Comparative analysis of the risks of hospitalisation and death associated with SARS-CoV-2 omicron (B.1.1.529) and delta (B.1.617.2) variants in England: a cohort study. Lancet. 399:1303–1312.

4. Nalbandian A, et al. 2021. Post-acute COVID-19 syndrome. Nat Med. 27:601–615.

5   Davis HE, McCorkell L, Vogel JM, Topol EJ. 2023. Long COVID: major findings, mechanisms and recommendations. *Nat Rev Microbiol*. 21:133–146.

6   Harris E. 2023. US survey: about 7% of adults, 1% of children have had long COVID. *JAMA*. 330:1516.

7   Ripa M, *et al*. 2022. "Vision loss" and COVID-19 infection: a systematic review and meta-analysis. *Vision (Basel)*. 6:60.

8   Hoffmann M, *et al*. 2020. SARS-CoV-2 cell entry depends on ACE2 and TMPRSS2 and is blocked by a clinically proven protease inhibitor. *Cell*. 181:271–280.e8.

9   Eriksen AZ, *et al*. 2021. SARS-CoV-2 infects human adult donor eyes and hESC-derived ocular epithelium. *Cell Stem Cell*. 28: 1205–1220.e7.

10 Menuchin-Lasowski Y, *et al*. 2022. SARS-CoV-2 infects and replicates in photoreceptor and retinal ganglion cells of human retinal organoids. *Stem Cell Reports*. 17:789–803.

11 Robbins SG, Hamel CP, Detrick B, Hooks JJ. 1990. Murine coronavirus induces an acute and long-lasting disease of the retina. *Lab Invest*. 62:417–426.

12 Robbins SG, Detrick B, Hooks JJ. 1991. Ocular tropisms of murine coronavirus (strain JHM) after inoculation by various routes. *Invest Ophthalmol Vis Sci*. 32:1883–1893.

13 Duran CS, Mayorga GD. 2021. The eye: "an organ that must not be forgotten in coronavirus disease 2019 (COVID-2019) pandemic". *J Optom*. 14:114–119.

14 Tao L, *et al*. 2016. Angiotensin-converting enzyme 2 activator diminazene aceturate prevents lipopolysaccharide-induced inflammation by inhibiting MAPK and NF-kappaB pathways in human retinal pigment epithelium. *J Neuroinflammation*. 13:35.

15 Henkind P, Hansen RI, Szalay J. 1979. Ocular circulation. In: Records RE, editors. *Physiology of the human eye and visual system*. Hagerstown (MD): Harper & Row. p. 98–155.

16 Hagman K, *et al*. 2022. Duration of SARS-CoV-2 viremia and its correlation to mortality and inflammatory parameters in patients hospitalized for COVID-19: a cohort study. *Diagn Microbiol Infect Dis*. 102:115595.

17 Casagrande M, *et al*. 2020. Detection of SARS-CoV-2 in human retinal biopsies of deceased COVID-19 patients. *Ocul Immunol Inflamm*. 28:721–725.

18 Araujo-Silva CA, *et al*. 2021. Presumed SARS-CoV-2 viral particles in the human retina of patients with COVID-19. *JAMA Ophthalmol*. 139:1015–1021.

19 Casagrande M, *et al*. 2022. Detection of SARS-CoV-2 genomic and subgenomic RNA in retina and optic nerve of patients with COVID-19. *Br J Ophthalmol*. 106:1313–1317.

20 Monu M, Ahmad F, Olson RM, Balendiran V, Singh PK. 2024. SARS-CoV-2 infects cells lining the blood-retinal barrier and induces a hyperinflammatory immune response in the retina via systemic exposure. *PLoS Pathog*. 20:e1012156.

21 Lakkaraju A, *et al*. 2020. The cell biology of the retinal pigment epithelium. *Prog Retin Eye Res*. 78:100846. doi:10.1016/j. preteyeres.2020.100846.

22 Sparrow JR, Hicks D, Hamel CP. 2010. The retinal pigment epithelium in health and disease. *Curr Mol Med*. 10:802–823.

23 Bhutto I, Lutty G. 2012. Understanding age-related macular degeneration (AMD): relationships between the photoreceptor/retinal pigment epithelium/Bruch's membrane/choriocapillaris complex. *Mol Aspects Med*. 33:295–317.

24 Trott M, Driscoll R, Pardhan S. 2022. The prevalence of sensory changes in post-COVID syndrome: a systematic review and meta-analysis. *Front Med (Lausanne)*. 9:980253.

25 Garcia LF. 2020. Immune response, inflammation, and the clinical Spectrum of COVID-19. *Front Immunol*. 11:1441.

26 Afzali B, Noris M, Lambrecht BN, Kemper C. 2022. The state of complement in COVID-19. *Nat Rev Immunol*. 22:77–84.

27 Kauppinen A, Paterno JJ, Blasiak J, Salminen A, Kaarniranta K. 2016. Inflammation and its role in age-related macular degeneration. *Cell Mol Life Sci*. 73:1765–1786.

28 Pennington KL, DeAngelis MM. 2016. Epidemiology of age-related macular degeneration (AMD): associations with cardiovascular disease phenotypes and lipid factors. *Eye Vis (Lond)*. 3:34.

29 Wong WL, *et al*. 2014. Global prevalence of age-related macular degeneration and disease burden projection for 2020 and 2040: a systematic review and meta-analysis. *Lancet Glob Health*. 2: e106–e116.

30 Cervia-Hasler C, *et al*. 2024. Persistent complement dysregulation with signs of thromboinflammation in active long COVID. *Science*. 383:eadg7942.

31 Hageman GS, *et al*. 2005. A common haplotype in the complement regulatory gene factor H (HF1/CFH) predisposes individuals to age-related macular degeneration. *Proc Natl Acad Sci U S A*. 102:7227–7232.

32 Klein RJ, *et al*. 2005. Complement factor H polymorphism in age-related macular degeneration. *Science*. 308:385–389.

33 Edwards AO, *et al*. 2005. Complement factor H polymorphism and age-related macular degeneration. *Science*. 308:421–424.

34 Zhou L, *et al*. 2020. ACE2 and TMPRSS2 are expressed on the human ocular surface, suggesting susceptibility to SARS-CoV-2 infection. *Ocul Surf*. 18:537–544.

35 Zhou L, *et al*. 2021. Expression of the SARS-CoV-2 receptor ACE2 in human retina and diabetes-implications for retinopathy. *Invest Ophthalmol Vis Sci*. 62:6.

36 Lutz C, Maher L, Lee C, Kang W. 2020. COVID-19 preclinical models: human angiotensin-converting enzyme 2 transgenic mice. *Hum Genomics*. 14:20.

37 Ma D, *et al*. 2020. Expression of SARS-CoV-2 receptor ACE2 and TMPRSS2 in human primary conjunctival and pterygium cell lines and in mouse cornea. *Eye (Lond)*. 34:1212–1219.

38 Xie X, *et al*. 2020. An infectious cDNA clone of SARS-CoV-2. *Cell Host Microbe*. 27:841–848.e3.

39 Al-Ani A, Sunba S, Hafeez B, Toms D, Ungrin M. 2020. In vitro maturation of retinal pigment epithelium is essential for maintaining high expression of key functional genes. *Int J Mol Sci*. 21: 6066.

40 Gamage AM, *et al*. 2020. Infection of human nasal epithelial cells with SARS-CoV-2 and a 382-nt deletion isolate lacking ORF8 reveals similar viral kinetics and host transcriptional profiles. *PLoS Pathog*. 16:e1009130.

41 Crawford KHD, *et al*. 2020. Protocol and reagents for pseudotyping lentiviral particles with SARS-CoV-2 spike protein for neutralization assays. *Viruses*. 12:513.

42 Dadras O, *et al*. 2022. The relationship between COVID-19 viral load and disease severity: a systematic review. *Immun Inflamm Dis*. 10:e580. https://doi.org/10.1002/iid3.580

43 Zhou Y, *et al*. 2023. A comprehensive SARS-CoV-2-human protein-protein interactome reveals COVID-19 pathobiology and potential host therapeutic targets. *Nat Biotechnol*. 41: 128–139.

44 Breitinger U, Farag NS, Sticht H, Breitinger HG. 2022. Viroporins: structure, function, and their role in the life cycle of SARS-CoV-2. *Int J Biochem Cell Biol*. 145:106185.

45 Shepley-McTaggart A, *et al*. 2021. SARS-CoV-2 envelope (E) protein interacts with PDZ-domain-2 of host tight junction protein ZO1. *PLoS One*. 16:e0251955.

46   Zhang Y, *et al.* 2021. The SARS-CoV-2 protein ORF3a inhibits fusion of autophagosomes with lysosomes. *Cell Discov.* 7:31.

47   Hazim RA, Volland S, Yen A, Burgess BL, Williams DS. 2019. Rapid differentiation of the human RPE cell line, ARPE-19, induced by nicotinamide. *Exp Eye Res.* 179:18–24.

48   Hazim RA, *et al.* 2022. Vitamin B3, nicotinamide, enhances mitochondrial metabolism to promote differentiation of the retinal pigment epithelium. *J Biol Chem.* 298:102286.

49   Rashid A, *et al.* 2016. RPE cell and sheet properties in normal and diseased eyes. *Adv Exp Med Biol.* 854:757–763.

50   Zhang J, *et al.* 2022. Understanding the role of SARS-CoV-2 ORF3a in viral pathogenesis and COVID-19. *Front Microbiol.* 13: 854567.

51   Zhang J, *et al.* 2021. Genome-Wide characterization of SARS-CoV-2 cytopathogenic proteins in the search of antiviral targets. *mBio.* 13:e0016922.

52   Hazim RA, Williams DS. 2018. Cell culture analysis of the phagocytosis of photoreceptor outer segments by primary mouse RPE cells. *Methods Mol Biol.* 1753:63–71.

53   Nandrot EF, *et al.* 2004. Loss of synchronized retinal phagocytosis and age-related blindness in mice lacking alphavbeta5 integrin. *J Exp Med.* 200:1539–1545.

54   Beaudoin CA, Hamaia SW, Huang CL, Blundell TL, Jackson AP. 2021. Can the SARS-CoV-2 spike protein bind integrins independent of the RGD sequence? *Front Cell Infect Microbiol.* 11: 765300.

55   Makowski L, Olson-Sidford W, W-Weisel J. 2021. Biological and clinical consequences of integrin binding via a Rogue RGD Motif in the SARS CoV-2 spike protein. *Viruses.* 13:146.

56   Finnemann SC. 2003. Focal adhesion kinase signaling promotes phagocytosis of integrin-bound photoreceptors. *EMBO J.* 22: 4143–4154.

57   Simons P, *et al.* 2021. Integrin activation is an essential component of SARS-CoV-2 infection. *Sci Rep.* 11:20398.

58   Nader D, Fletcher N, Curley GF, Kerrigan SW. 2021. SARS-CoV-2 uses major endothelial integrin alphavbeta3 to cause vascular dysregulation in-vitro during COVID-19. *PLoS One.* 16:e0253347.

59   Liu J, Lu F, Chen Y, Plow E, Qin J. 2022. Integrin mediates cell entry of the SARS-CoV-2 virus independent of cellular receptor ACE2. *J Biol Chem.* 298:101710.

60   V'Kovski P, Kratzel A, Steiner S, Stalder H, Thiel V. 2021. Coronavirus biology and replication: implications for SARS-CoV-2. *Nat Rev Microbiol.* 19:155–170.

61   Esteve-Rudd J, Lopes VS, Jiang M, Williams DS. 2014. In vivo and in vitro monitoring of phagosome maturation in retinal pigment epithelium cells. *Adv Exp Med Biol.* 801:85–90.

62   Shi G, *et al.* 2008. Control of chemokine gradients by the retinal pigment epithelium. *Invest Ophthalmol Vis Sci.* 49:4620–4630.

63   Holtkamp GM, Kijlstra A, Peek R, de Vos AF. 2001. Retinal pigment epithelium-immune system interactions: cytokine production and cytokine-induced changes. *Prog Retin Eye Res.* 20: 29–48.

64   Wang K, Guan T, Cheresh DA, Nemerow GR. 2000. Regulation of adenovirus membrane penetration by the cytoplasmic tail of integrin beta5. *J Virol.* 74:2731–2739.

65   Wickham TJ, Mathias P, Cheresh DA, Nemerow GR. 1993. Integrins alpha v beta 3 and alpha v beta 5 promote adenovirus internalization but not virus attachment. *Cell.* 73:309–319.

66   Wang S, *et al.* 2020. Integrin alphavbeta5 internalizes Zika virus during neural stem cells infection and provides a promising target for antiviral therapy. *Cell Rep.* 30:969–983.e4.

67   Dedoni S, *et al.* 2022. K18- and CAG-hACE2 transgenic mouse models and SARS-CoV-2: implications for neurodegeneration research. *Molecules.* 27:4142.

68   Burgos-Blasco B, *et al.* 2022. Optic nerve and macular optical coherence tomography in recovered COVID-19 patients. *Eur J Ophthalmol.* 32:628–636.

69   Fenrich M, *et al.* 2020. SARS-CoV-2 dissemination through peripheral nerves explains multiple organ injury. *Front Cell Neurosci.* 14:229.

70   Castanheira FVS, *et al.* 2023. Intravital imaging of three different microvascular beds in SARS-CoV-2-infected mice. *Blood Adv.* 7: 4170–4181.

71   Liu YC, Ang M, Ong HS, Wong TY, Mehta JS. 2020. SARS-CoV-2 infection in conjunctival tissue. *Lancet Respir Med.* 8:e57.

72   Davis G, Li K, Thankam FG, Wilson DR, Agrawal DK. 2022. Ocular transmissibility of COVID-19: possibilities and perspectives. *Mol Cell Biochem.* 477:849–864.

73   Sawant OB, *et al.* 2021. Prevalence of SARS-CoV-2 in human post-mortem ocular tissues. *Ocul Surf.* 19:322–329.

74   Jackson RM, *et al.* 2022. Conjunctival epithelial cells resist productive SARS-CoV-2 infection. *Stem Cell Reports.* 17:1699–1713.

75   Peng S, *et al.* 2024. CRB1-associated retinal degeneration is dependent on bacterial translocation from the gut. *Cell.* 187: 1387–1401.e13.

76   Wang L, *et al.* 2023. Cell type dependent stability and virulence of a recombinant SARS-CoV-2, and engineering of a propagation deficient RNA replicon to analyze virus RNA synthesis. *Front Cell Infect Microbiol.* 13:1268227.

77   Odenwald MA, *et al.* 2017. ZO-1 interactions with F-actin and occludin direct epithelial polarization and single lumen specification in 3D culture. *J Cell Sci.* 130:243–259.

78   Nagaoka K, Udagawa T, Richter JD. 2012. CPEB-mediated ZO-1 mRNA localization is required for epithelial tight-junction assembly and cell polarity. *Nat Commun.* 3:675.

79   Javorsky A, Humbert PO, Kvansakul M. 2021. Structural basis of coronavirus E protein interactions with human PALS1 PDZ domain. *Commun Biol.* 4:724.

80   Shepley-McTaggart A, *et al.* 2021. SARS-CoV-2 Envelope (E) protein interacts with PDZ-domain-2 of host tight junction protein ZO1. *PLoS One.* 16(6):e0251955. https://doi.org/10.1371/journal.pone.0251955.

81   Caillet-Saguy C, *et al.* 2021. Host PDZ-containing proteins targeted by SARS-CoV-2. *FEBS J.* 288:5148–5162.

82   Naylor A, Hopkins A, Hudson N, Campbell M. 2019. Tight junctions of the outer blood retina barrier. *Int J Mol Sci.* 21:211.

83   Sen S, *et al.* 2022. Retinal manifestations in patients with SARS-CoV-2 infection and pathogenetic implications: a systematic review. *Int Ophthalmol.* 42:323–336.

84   Ferrington DA, Sinha D, Kaarniranta K. 2016. Defects in retinal pigment epithelial cell proteolysis and the pathology associated with age-related macular degeneration. *Prog Retin Eye Res.* 51: 69–89.

85   Schoeman D, Fielding BC. 2019. Coronavirus envelope protein: current knowledge. *Virol J.* 16:69.

86   Datta S, Cano M, Ebrahimi K, Wang L, Handa JT. 2017. The impact of oxidative stress and inflammation on RPE degeneration in non-neovascular AMD. *Prog Retin Eye Res.* 60:201–218.

87   Cabrera-Garcia D, Bekdash R, Abbott GW, Yazawa M, Harrison NL. 2021. The envelope protein of SARS-CoV-2 increases intra-Golgi pH and forms a cation channel that is regulated by pH. *J Physiol.* 599:2851–2868.

88 Inana G, *et al.* 2018. RPE phagocytic function declines in age-related macular degeneration and is rescued by human umbilical tissue derived cells. *J Transl Med*. 16:63.

89 Gal A, *et al.* 2000. Mutations in MERTK, the human orthologue of the RCS rat retinal dystrophy gene, cause retinitis pigmentosa. *Nat Genet*. 26:270–271.

90 Guziewicz KE, *et al.* 2017. Bestrophinopathy: an RPE-photoreceptor interface disease. *Prog Retin Eye Res*. 58:70–88.

91 George SM, Lu F, Rao M, Leach LL, Gross JM. 2021. The retinal pigment epithelium: development, injury responses, and regenerative potential in mammalian and non-mammalian systems. *Prog Retin Eye Res*. 85:100969.

92 Armento A, Ueffing M, Clark SJ. 2021. The complement system in age-related macular degeneration. *Cell Mol Life Sci*. 78: 4487–4505.

93 Ramlall V, *et al.* 2020. Immune complement and coagulation dysfunction in adverse outcomes of SARS-CoV-2 infection. *Nat Med*. 26:1609–1615.

94 Gold B, *et al.* 2006. Variation in factor B (BF) and complement component 2 (C2) genes is associated with age-related macular degeneration. *Nat Genet*. 38:458–462.

95 Maller JB, *et al.* 2007. Variation in complement factor 3 is associated with risk of age-related macular degeneration. *Nat Genet*. 39:1200–1201.

96 Narendra U, Pauer GJ, Hagstrom SA. 2009. Genetic analysis of complement factor H related 5, CFHR5, in patients with age-related macular degeneration. *Mol Vis*. 15:731–736.

97 Jabs DA, *et al.* 2015. Prevalence of intermediate-stage age-related macular degeneration in patients with acquired immunodeficiency syndrome. *Am J Ophthalmol*. 159:1115–1122.e1.

98 Jabs DA, Van Natta ML, Pak JW, Danis RP, Hunt PW. 2017. Incidence of intermediate-stage age-related macular degeneration in patients with acquired immunodeficiency syndrome. *Am J Ophthalmol*. 179:151–158.

99 Jabs DA, *et al.* 2024. Association of intermediate-stage age-related macular degeneration with plasma inflammatory biomarkers in persons with AIDS. *Ophthalmol Sci*. 4:100437.

100 Curcio CA, Medeiros NE, Millican CL. 1996. Photoreceptor loss in age-related macular degeneration. *Invest Ophthalmol Vis Sci*. 37: 1236–1249.

101 Hartmann KI, *et al.* 2011. Scanning laser ophthalmoscope imaging stabilized microperimetry in dry age-related macular degeneration. *Retina*. 31:1323–1331.

102 Iwama D, *et al.* 2010. Relationship between retinal sensitivity and morphologic changes in eyes with confluent soft drusen. *Clin Exp Ophthalmol*. 38:483–488.

103 Sulzbacher F, *et al.* 2012. Correlation of SD-OCT features and retinal sensitivity in neovascular age-related macular degeneration. *Invest Ophthalmol Vis Sci*. 53:6448–6455.

104 Handa JT. in press. Pathobiology of non-neovascular age-related macular degeneration. In: D'Amore P, editor. *Encyclopedia of the eye*. 2nd ed. Oxford, UK: Elsevier Press.